JOM 23706

Structures and Mössbauer spectra of phosphido-bridged heterobimetallic complexes $CpFe(CO)_2(\mu\text{-}PPh_2)W(CO)_5$ and $CpFe(CO)(\mu\text{-}CO)(\mu\text{-}PPh_2)W(CO)_4$

Shin-Guang Shyu, Pei-Jung Lin, Teng-Yuan Dong and Yuh-Shang Wen

Institute of Chemistry, Academia Sinica, Taipei (Taiwan)

(Received December 18, 1992; in revised form March 27, 1993)

Abstract

Structures of non metal–metal bonded phosphido-bridged heterobimetallic complexes, including $CpFe(CO)_2(\mu\text{-}PPh_2)W(CO)_5$ (**1-W**) and metal–metal bonded $CpFe(CO)(\mu\text{-}CO)(\mu\text{-}PPh_2)W(CO)_4$ (**2**), were determined by a single crystal X-ray diffraction study. In **1-W**, the long distance between Fe and W indicates no metal–metal bond to exist. In **2**, a Fe–W bond with bond length 2.851 Å and a semibridging carbonyl with W–C–O angle 153° were observed. Mössbauer spectra of **1-W** and **2** were taken at 77 K. Isomer shifts of **1-W** and **2** were -0.0203 mm s^{-1} and 0.1917 mm s^{-1} respectively.

1. Introduction

A metal–metal bonded phosphido-bridged binuclear complex can be generated by the removal of one CO from the corresponding precursor, which does not have a metal–metal bond [1]. The coordination site previously occupied by the removed CO is replaced by the dative metal–metal bond originated from the adjacent metal in the dimer. The metal–metal bonded complex formed has two possible structures, one with bridging CO (**A**) and the other without (**B**). These two structures have been proposed to exist as isomers in solution [2].

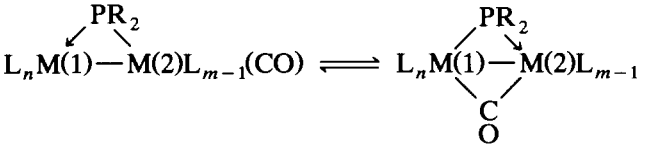

(**A**) (**B**)

Many complexes, as determined by X-ray diffraction, have structure **A** [3]. Only a few homobimetallic metal–metal bonded monophosphido-bridged Fe complexes with the structure **B** have been reported [4]. Structures of heterobimetallic phosphido-bridged complexes, which contain semibridging or bridging CO ligands, have also been determined [5].

Recently, we have published the procedure for the synthesis of $CpFe(CO)(\mu\text{-}CO)(\mu\text{-}PPh_2)W(CO)_4$ (**2**) through the removal of one CO by photolysis from the corresponding precursor $CpFe(CO)_2(\mu\text{-}PPh_2)W(CO)_5$ (**1-W**) [6]. Here we report the X-ray crystal structures and Mössbauer spectra of the complex **2**. The X-ray crystal structure and Mössbauer spectrum of **1-W** are also reported for comparison.

2. Experimental section

2.1. Preparation of complex

Complexes **1-W** and **2** were prepared according to literature procedures [6].

2.2. Structural determination of 1-W

A yellowish brown, needlelike crystal (0.38 × 0.34 × 0.41 mm), which was grown by slow diffusion of hexanes to the saturated benzene solution of **1-W** at −15°C under nitrogen, was used for data collection at 298 K. Cell dimensions and space group data were obtained by standard methods on an Enraf–Nonius CAD4 diffractometer. The ω–2θ scan technique was used to record the intensities for all the reflections

Correspondence to: Dr. S.-G. Shyu.

0022-328X/93/$6.00

with $1° < 2\theta < 49.8°$. Absorption corrections were made with empirical ψ rotation. Of the 4137 independent intensities, there were 3177 with $F_o > 2.5\sigma(F_o^2)$, where $\sigma(F_o^2)$ were estimated from counting statistics. These data were used in the final refinement of the structural parameters. The X-ray crystal data are summarized in Table 1.

A three-dimensional Patterson synthesis was used to determine the heavy-atom positions, which phased the data sufficiently well to permit location of the remaining non-hydrogen atoms from Fourier synthesis. All non-hydrogen atoms were refined anisotropically. During the final cycles of refinement, fixed hydrogen contributions with C–H bond lengths fixed at 1.08 Å were applied. The final positional parameters for all atoms are listed in Table 2, and the selected bond distances and angles are given in Table 3. The thermal parameters and observed calculated structure factors are provided in the supplementary material.

2.3. Structural determination of 2

Dark brown needlelike crystals of **2** were grown by slow diffusion of hexanes to the saturated benzene solution of **2** at −15°C. A single crystal of complex **2** (0.06 × 0.06 × 0.39 mm) was sealed within a Pyrex capillary under dry nitrogen in the glove box and mounted on the diffractometer. Upon exposure to air, these crystals decomposed gradually. Data were collected to the 2θ value of 49.8°. The data were also corrected for absorption with an empirical ψ rotation. Of the 3936 independent intensities, there were 1460 with $F_o > 2.5\sigma(F_o^2)$. These data were used in the final refinement of the structural parameters. The X-ray crystal data are summarized in Table 1.

Structure refinement was carried out in the similar manner as described for **1-W** except that some carbon atoms were refined isotropically. Atomic coordinates are listed in Table 4. The selected bond distances and angles are given in Table 3. Thermal parameters as well as observed and calculated structure factors are available as supplementary material.

TABLE 1. Crystal and intensity collection data for **1-W** and **2**

Molecular formula	$C_{24}H_{15}FeO_7PW$	$C_{23}H_{15}FeO_6PW$
Mol. wt.	686.04	658.03
Crystal system	Monoclinic	Monoclinic
Space group	$P2_1/n$	$P2_1/n$
a (Å)	9.1782(13)	9.183(4)
b (Å)	17.5546(15)	17.877(4)
c (Å)	14.7113(18)	14.249(3)
α (deg)	–	–
β (deg)	94.949(11)	106.38(3)
γ (deg)	–	–
V (Å^3)	2361.4(5)	2244.3(11)
ρ (calc.) (mg m^{-3})	1.930	1.948
Z	4	4
Crystal dimensions (mm)	0.38×0.34×0.41	0.06×0.06×0.39
Absolute coefficient μ (Mo K$_\alpha$) (mm^{-1})	5.69	5.98
Temperature	Room temperature	Room temperature
Radiation	Mo K$_\alpha$ λ = 0.70930 Å	Mo K$_\alpha$ λ = 0.70930 Å
2θ range	49.8°	49.8°
Scan type	$2\theta-\omega$	$2\theta-\omega$
No. of reflections	6911	4197
No. of observed reflections	3177 ($> 2.5\sigma$)	1460 ($> 2.5\sigma$)
Variables	367	225
R	0.025	0.050
R_w	0.027	0.051
S	1.33	1.16
ΔF(e/Å^3)	< 1.190	< 0.790
$(\Delta/\sigma)_{max}$	0.005	0.021

2.4. ^{57}Fe Mössbauer measurements

^{57}Fe Mössbauer measurements were made on a constant-acceleration-type instrument. The source, which originally consisted of 35 mCi of ^{57}Co diffused into a 12 μm rhodium matrix, was connected to a Ranger Scientific Model VT-900 velocity transducer. Computer fittings of the ^{57}Fe Mössbauer data to Lorentzian lines were carried out with a modified version of a previously reported program [7]. Velocity calibrations were made by use of a 99.99% pure 10 μm iron foil. Typical line widths for all three pairs of iron lines fell in the range of 0.25–0.28 mm s^{-1}. Isomer shifts are reported with respect to iron foil at 300 K but are uncorrected for temperature-dependent, second-order Doppler effects. It should be noted that the isomer shifts illustrated in the figures are plotted as experimentally obtained; tabulated data should be consulted.

3. Results and discussion

3.1. Molecular structures of 1-W and 2

After the structures of the Cr and Mo analogues of **1-W** had been determined [6], we undertook a diffraction study of these complexes to provide the basis for an unambiguous comparison of various structural parameters with those of metal–metal bonded CpFe(CO)(μ-CO)(μ-PPh$_2$)W(CO)$_4$ (**2**).

An ORTEP drawing of the molecular structure of **1-W** is shown in Fig. 1. The long distance between Fe and W (4.2110 Å) in **1-W** indicates that no metal–metal bond exists. We believe the CpFe(CO)$_2$PPh$_2$ fragment as a metallophosphine ligand with the phosphorus atom donating two electrons to W. Thus both the Fe and W atoms could be saturated coordinatively with 18 va-

lence electrons. The polyhedron around the tungsten was considered as distorted octahedron. The least square plane consists with P, C(3), C(4), C(5), W can be considered as the equatorial plane of the octahedron [8*]. Two carbonyl ligands, C(1)O(1) and C(2)O(2), occupied the axial position with the C(1)–W–C(2) angle of 174.51°.

The structure of **1**-W was similar to those of its Cr and Mo analogues: $CpFe(CO)_2(\mu\text{-}PPh_2)Cr(CO)_5$, **1**-Cr, and $CpFe(CO)_2(\mu\text{-}PPh_2)Mo(CO)_5$, **1**-Mo. Selected bond lengths and bond angles for these compounds are listed in Table 5. In all three complexes, the Fe–P distances were almost the same. For the distance between M–P (M = Cr, Mo, W), it was longer for Fe–W and Fe–Mo than for Fe–Cr owing to the covalent radii of Mo and W being larger than those of Cr.

* Reference number with an asterisk indicates a note in the list of references.

We removed one CO by photolysis from **1**-W to give complex **2**. An ORTEP drawing of the molecular structure of **2** is shown in Fig. 2. The metal–metal bond distance between the Fe and the W atoms in **2** was 2.851(4) Å, which falls in the range reported for some Fe–W mixed-metal clusters with bridging phosphido group, including $[WFe_2(\mu_3\text{-}CC_6H_4Me\text{-}4)(\mu\text{-}PPh_2)_2(CO)_6(\eta\text{-}C_5H_5)]\cdot 0.5CH_2Cl_2$ (2.783(1) Å), $[WFe_2(\mu_3\text{-}OCH_2C_6H_4Me\text{-}4)(\mu\text{-}PPh_2)_2(CO)_5(\eta\text{-}C_5H_5)]$ (2.712(1) Å), $[WFe_2(\mu_3\text{-}OCH_2C_6H_4Me\text{-}4)(\mu\text{-}PPh_2)_2(CO)_6(PPh_2H)(\eta\text{-}C_5H_5)]\cdot CH_2Cl_2$ (2.940(1) Å), $[WFe_2(\mu_3\text{-}CC_6H_4Me\text{-}4)(\mu\text{-}H)(\mu\text{-}PEt_2)(CO)_6(PEt_2H)(\eta\text{-}C_5H_5)]\cdot Et_2O$ (2.830(1) Å) [9], and $[WFe_2(\mu_3\text{-}CC_6H_4Me\text{-}4)\{(\mu\text{-}C(O)C(Me)CHMe\}(\mu\text{-}PEt_2)(CO)_5(\eta\text{-}C_5H_5)]$(2.808(1) Å) [10]. The Fe–W distance in **2** was also similar to those in several bridged dimetallic complexes, including $[WFe\{(\mu\text{-}C(C_6H_4Me\text{-}4)C(Me)C(Me)\}(CO)_5(\eta\text{-}C_5H_5)]$ (2.720(1) Å) [11], $[WFe\{(\mu\text{-}C(C_6H_4Me\text{-}4)C(Et)C(Me)\}(\mu\text{-}CO)(CO)_3(\eta\text{-}C_5Me_5)]$ (2.729(1) Å) [12] and $[WFe\{\mu\text{-}C(Et)C(Et)C(H)CH$-

TABLE 2. Atomic coordinates and isotropic thermal parameters (Å^2) for **1**-W

Atom	x	y	z	B_{iso}
W	0.29357(2)	0.11551(1)	0.01737(1)	2.68(1)
Fe	0.04987(8)	0.25201(5)	0.18440(6)	3.26(3)
P	0.27708(14)	0.20449(8)	0.15579(9)	2.65(5)
O1	0.2641(5)	0.2406(3)	−0.1367(3)	5.5(2)
O2	0.3176(5)	−0.0285(3)	0.1497(3)	5.5(2)
O3	0.6379(4)	0.1420(3)	0.0462(3)	5.2(2)
O4	0.3287(5)	0.0090(3)	−0.1502(3)	5.2(2)
O5	−0.0490(5)	0.0917(3)	−0.0145(4)	6.6(3)
O6	0.1410(6)	0.2706(3)	0.3764(3)	7.0(3)
O7	−0.0781(6)	0.1032(3)	0.2074(4)	6.9(3)
C1	0.2737(6)	0.1982(3)	−0.0781(4)	3.6(3)
C2	0.3103(6)	0.0233(4)	0.1051(4)	3.7(3)
C3	0.5153(6)	0.1316(3)	0.0366(4)	3.0(2)
C4	0.3162(6)	0.0462(3)	−0.0876(4)	3.5(2)
C5	0.0732(6)	0.1012(3)	−0.0018(4)	3.7(3)
C6	0.1077(7)	0.2629(4)	0.3004(5)	4.7(3)
C7	−0.0253(6)	0.1603(4)	0.1976(4)	4.1(3)
C8	0.0516(8)	0.3152(4)	0.0636(5)	4.9(3)
C9	−0.0819(8)	0.2760(5)	0.0640(5)	5.4(4)
C10	−0.1505(8)	0.3022(5)	0.1397(6)	5.8(4)
C11	−0.0618(9)	0.3560(5)	0.1843(6)	5.9(4)
C12	0.0661(8)	0.3639(4)	0.1397(6)	5.5(4)
C21	0.3662(6)	0.1515(3)	0.2554(3)	2.8(2)
C22	0.2869(7)	0.1081(4)	0.3130(4)	3.9(3)
C23	0.3565(8)	0.0627(4)	0.3783(5)	4.5(3)
C24	0.5063(8)	0.0578(4)	0.3880(5)	4.6(3)
C25	0.5855(7)	0.1003(4)	0.3317(4)	4.2(3)
C26	0.5144(6)	0.1473(4)	0.2665(4)	3.7(3)
C31	0.3925(5)	0.2911(3)	0.1565(4)	2.9(2)
C32	0.4282(6)	0.3313(4)	0.2370(5)	4.0(3)
C33	0.5015(7)	0.4002(4)	0.2368(5)	4.9(3)
C34	0.5424(8)	0.4305(4)	0.1559(6)	5.0(4)
C35	0.5101(7)	0.3914(4)	0.0758(5)	5.1(3)
C36	0.4364(7)	0.3210(4)	0.0767(5)	4.1(3)

$(C_6H_4Me\text{-}4)](\mu\text{-}CO)(CO)_4(\eta\text{-}C_5Me_5)]$ (2.798(1) Å) [13].

In addition to the μ-PPh_2, the CO, and the Cp ligands on Fe, the W–Fe dative bond could serve as the fourth ligand, which donated two electrons to Fe. Consistent with this viewpoint was that the W–Fe vector bisected an edge of the distorted tungsten octahedron. The W atom lay on the least square plane consisting P, C(3), C(4), C(5) [14*]. The W–Fe vector was 8.33° off the plane. The W–Fe bond could donate

TABLE 3. Selected bond lengths (Å) and bond angles (°) in complexes **1-W** and **2**

1-W		**2**	
Bond lengths			
W···Fe	4.2110(9)	W–Fe	2.851(3)
W–P	2.5813(14)	W–P	2.463(7)
W–C(1)	2.017(6)	W–C(1)	2.05(3)
W–C(2)	2.068(6)	W–C(2)	2.033(24)
W–C(3)	2.050(6)	W–C(3)	1.99(3)
W–C(4)	1.991(6)	W–C(4)	1.93(3)
W–C(5)	2.034(5)	W–C(5)	2.109(23)
Fe–P	2.3181(15)	Fe–P	2.204(6)
Fe–C(6)	1.753(8)	Fe–C(5)	2.232(24)
Fe–C(7)	1.768(7)	Fe–C(6)	1.82(3)
O(1)–C(1)	1.136(8)	O(1)–C(1)	1.10(3)
O(2)–C(2)	1.120(8)	O(2)–C(2)	1.18(3)
O(3)–C(3)	1.137(7)	O(3)–C(3)	1.18(3)
O(4)–C(4)	1.143(7)	O(4)–C(4)	1.20(4)
O(5)–C(5)	1.133(7)	O(5)–C(5)	1.17(3)
O(6)–C(6)	1.141(9)	O(6)–C(6)	1.07(3)
O(7)–C(7)	1.129(8)		
Bond angles			
P–W–C(1)	96.09(17)	P–W–C(1)	96.0(10)
P–W–C(2)	89.27(16)	P–W–C(2)	84.4(9)
P–W–C(3)	86.15(15)	P–W–C(3)	91.6(8)
P–W–C(4)	177.32(16)	P–W–C(4)	174.2(7)
P–W–C(5)	93.37(15)	P–W–C(5)	98.2(6)
P–Fe–C(6)	93.34(19)	P–Fe–C(5)	102.7(6)
P–Fe–C(7)	90.80(19)	P–Fe–C(6)	94.4(8)
W–C(1)–O(1)	174.8(5)	W–C(1)–O(1)	175(3)
W–C(2)–O(2)	177.2(5)	W–C(2)–O(2)	175(3)
W–C(3)–O(3)	178.4(5)	W–C(3)–O(3)	175.5(22)
W–C(5)–O(5)	177.9(5)	W–C(5)–O(5)	153.3(18)
Fe–C(6)–O(6)	177.8(5)	Fe–C(5)–O(5)	124.7(16)
Fe–C(7)–O(7)	177.2(6)	Fe–C(6)–O(6)	176.8(22)
		W–C(5)–Fe	82.0(9)
W–P–C(21)	105.45(16)	W–P–C(21)	119.0(7)
W–P–C(31)	115.37(17)	W–P–C(31)	125.0(8)
Fe–P–C(21)	112.18(16)	Fe–P–C(21)	119.5(7)
Fe–P–C(31)	103.12(16)	Fe–P–C(31)	119.8(6)
C(21)–P–C(31)	101.13(24)	C(21)–P–C(31)	99.5(10)
W–P–Fe	118.42(6)	W–P–Fe	75.06(22)
		Fe–W–P	48.33(14)
		Fe–W–C(5)	50.9(6)
		W–Fe–P	56.60(18)
		W–Fe–C(6)	96.8(8)

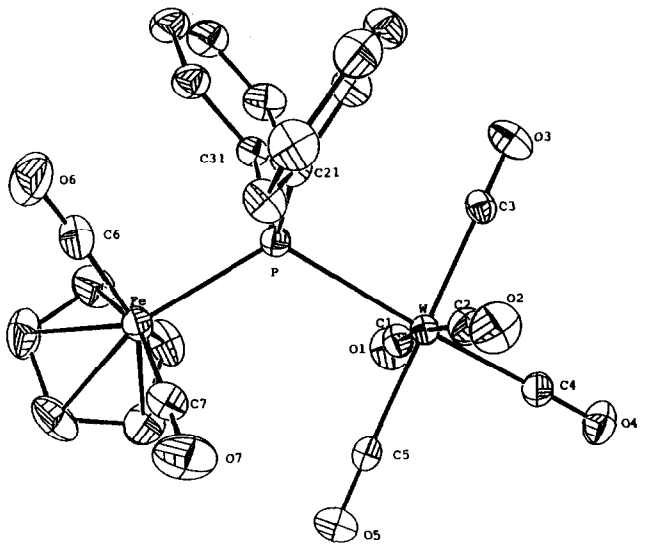

Fig. 1. ORTEP drawing of **1-W**. Hydrogen atoms are omitted.

TABLE 4. Atomic coordinates and isotropic thermal parameters (Å^2) for **2**

Atom	*x*	*y*	*z*	B_{iso}
W	0.77418(11)	0.94697(6)	0.63591(7)	2.82(5)
Fe	0.93531(36)	0.88894(21)	0.82267(23)	2.86(16)
P	0.7969(6)	0.8191(4)	0.7030(4)	2.7(3)
O(1)	1.0876(19)	0.9435(15)	0.5860(13)	6.7(12)
O(2)	0.4537(19)	0.9528(13)	0.6851(13)	5.9(11)
O(3)	0.6331(24)	0.8862(11)	0.4202(12)	6.7(12)
O(4)	0.7078(23)	1.1084(11)	0.5493(14)	6.7(12)
O(5)	0.9086(17)	1.0594(10)	0.8143(11)	4.2(8)
O(6)	0.7009(22)	0.9097(11)	0.9189(13)	6.4(12)
C(1)	0.9794(33)	0.9474(20)	0.6049(20)	5.5(18)
C(2)	0.5728(25)	0.9481(18)	0.6690(16)	3.6(13)
C(3)	0.6797(28)	0.9095(15)	0.5010(19)	4.3(6)
C(4)	0.7345(26)	1.0459(18)	0.5798(16)	4.2(14)
C(5)	0.8739(26)	1.0049(14)	0.7673(16)	3.3(12)
C(6)	0.7848(28)	0.9017(14)	0.8809(18)	3.7(5)
C(7)	1.1607(24)	0.9264(13)	0.8433(19)	3.8(12)
C(8)	1.1468(29)	0.8545(17)	0.8118(18)	4.4(6)
C(9)	1.1083(29)	0.8096(14)	0.8776(22)	5.1(14)
C(10)	1.0870(25)	0.8588(19)	0.9572(17)	4.3(15)
C(11)	1.1229(25)	0.9289(17)	0.9303(19)	4.3(14)
C(21)	0.6281(26)	0.7729(12)	0.7176(16)	3.0(12)
C(22)	0.6220(29)	0.7413(15)	0.8065(18)	4.5(6)
C(23)	0.4857(31)	0.7038(16)	0.8084(19)	5.2(6)
C(24)	0.3701(29)	0.7000(16)	0.7267(20)	4.9(6)
C(25)	0.3712(34)	0.7335(18)	0.6466(22)	6.2(7)
C(26)	0.4967(31)	0.7717(15)	0.6342(18)	4.8(6)
C(31)	0.8841(21)	0.7406(12)	0.6573(16)	2.7(11)
C(32)	0.8914(26)	0.6710(14)	0.6979(16)	3.4(5)
C(33)	0.9545(25)	0.6111(13)	0.6600(16)	3.5(5)
C(34)	0.9933(23)	0.6176(12)	0.5751(14)	2.5(4)
C(35)	0.9843(24)	0.6855(13)	0.5317(14)	2.9(5)
C(36)	0.9252(23)	0.7472(12)	0.5689(15)	2.2(4)

TABLE 5. Selected bond lengths (Å) and angles (°) in complexes 1-M (M = Cr, Mo, W)

	1-Cr	1-Mo	1-W
Bond lengths			
M–Fe	4.1278(10)	4.2250(6)	4.2110(9)
M–P	2.4636(13)	2.5952(10)	2.5815(14)
Fe–P	2.3214(13)	2.3158(11)	2.3180(15)
Bond angles			
M–P–Fe	119.20(5)	118.59(4)	118.42(6)
M–C(1)–O(1)	173.5(4)	174.3(3)	174.9(5)
M–C–O(ave.)	176.7(9)	177.4(1)	177.7(0)

an electron pair from one of the filled t_{2g} orbitals of the W atom to the adjacent Fe atom [15].

The W–C(5)–O(5) angle of 153.3° in **2** indicates a semibridging carbonyl. This assignment agrees with the result that the W–C(5) bond (2.109(23) Å) is shorter than the Fe–C(5) bond (2.232(24) Å) despite the covalent radius of W being larger than that of Fe. If the CO were to be bonded to Fe and W symmetrically, the Fe–C(5) bond length should be shorter than the W–C(5) bond length similar to $[FeW\{\mu\text{-}CH(C_6H_4Me\text{-}4)\}(\mu\text{-}\sigma:\eta^5\text{-}C_2B_9H_8Me_2)(\mu\text{-}CO)(CO)_5]^{-1}$ [16] having a smaller bond distance from the carbon of the bridging carbonyl group to Fe atom (2.021(4) Å) than to the W atom (2.172(5) Å).

Formation of **2** by removal of CO from Fe in **1-W** could have brought the P, C(3), C(4), C(5) plane of **1-W** close to the iron fragment. The filled t_{2g} orbital of W atom came close to the Fe atom and served as the incoming ligand to occupy the empty site left by the CO that had been removed. Because of the steric hindrance among the phosphido-bridge, the CO(5) ligand, and the ligands on iron, the W octahedral was distorted such that the angle of P–W–C(5) was enlarged and the angle between the Fe–W vector and the octahedral plane was increased from 6.03° in **1-W** to 8.33° in **2** [8*,14*]. The formation of the metal–metal bond that brought two metals close to each other also resulted in the reduction of the W–P–Fe angle from 118.42° in **1-W** to 75.06° in **2**. As the result, the distances of W–P and Fe–P in **2** were also shorter than the corresponding distances in **1-W**. For the same reason, the distance between the Fe atom and the CO(5) ligand on W atom was reduced and the release of electron of the filled d orbital of iron to the π^* orbital of CO(5) ligand became possible and thus resulted in the formation of the semibridging carbonyl [17].

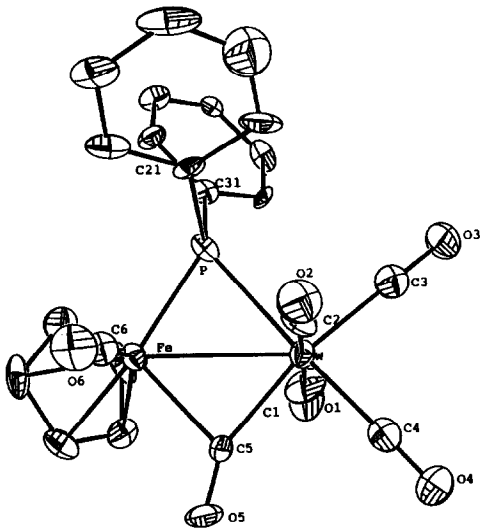

Fig. 2. ORTEP drawing of **2**. Hydrogen atoms are omitted.

3.2. Reconsideration of the fluxional behaviour of 2

We reported that the IR spectra of heterobimetallic metal–metal bonded phosphido-bridged complex $CpFe(CO)(\mu\text{-}CO)(\mu\text{-}PPh_2)W(CO)_4$ (**2**) in THF [18*] did not show any absorption corresponding to bridging or semibridging CO ligands [6]. Nevertheless, the IR

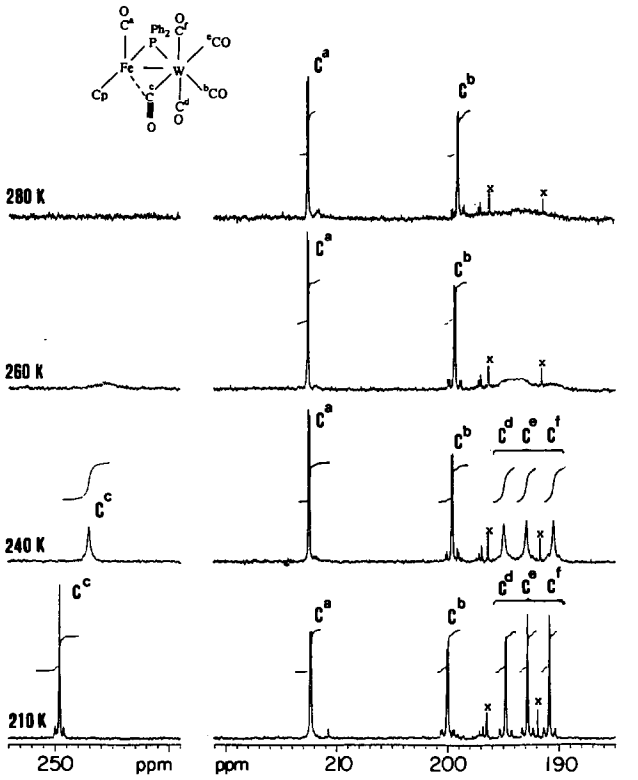

Fig. 3. Variable temperature $^{13}C\{^1H\}$ NMR spectrum of **2** in CD_2Cl_2. Only carbonyl region is shown. Signals due to impurities are marked x.

spectrum of the complex in the solid state showed an absorption at 1836 cm^{-1}, which indicated the existence of a semibridging CO. We also obtained variable ^{13}C NMR spectra of **2** in CD_2Cl_2 for the observation of the possible bridging CO signal at low temperatures (Fig. 3). At 210 K, an iron CO signal c^a and five tungsten CO signals (c^b, c^c, c^d, c^e, c^f) with c^c at 251 ppm belonging to the semibridging CO were observed. Our assignment was on the basis of the knowledge that a bridging CO or semibridging CO usually has a resonance that is relatively downfield compared with that of a terminal CO. At higher temperature, signals of three *cis* CO (terminal CO on the W occupying position *cis* to the P atom) ligands (c^f, c^d, c^e) and the semibridging CO (c^c) were broader, and the *trans* CO signal (c^b) and the iron CO signal (c^a) remained intact. Thus the presence of the semibridging CO of complex **2** in solution at low temperature was confirmed.

The exchange of the semibridging carbonyl ligand and the other three *cis* CO ligands in complex **2** may go through the rotation of the W–P bond (Scheme 1). This rotation required the breaking and reforming of the metal–metal dative bond. Breakage of the metal–metal bond in phosphido-bridged complexes is usually accompanied by an upfield shift of the ^{31}P NMR resonance [19]. Results from our variable temperature ^{31}P NMR experiments on **2** did not show any change of the resonance position. This may be due to the short-lived intermediate **c′** of the exchange reaction.

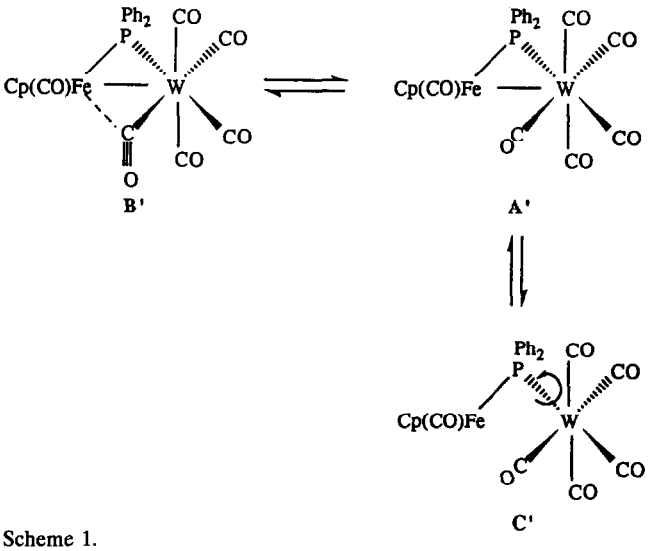

Scheme 1.

The absence of an observable bridging CO absorption IR of this complex in solution (CH_2Cl_2 and THF) at room temperature could be rationalized as follows: at low temperature, complex **B′** is the dominant species. At room temperature, complex **A′**, which is in rapid

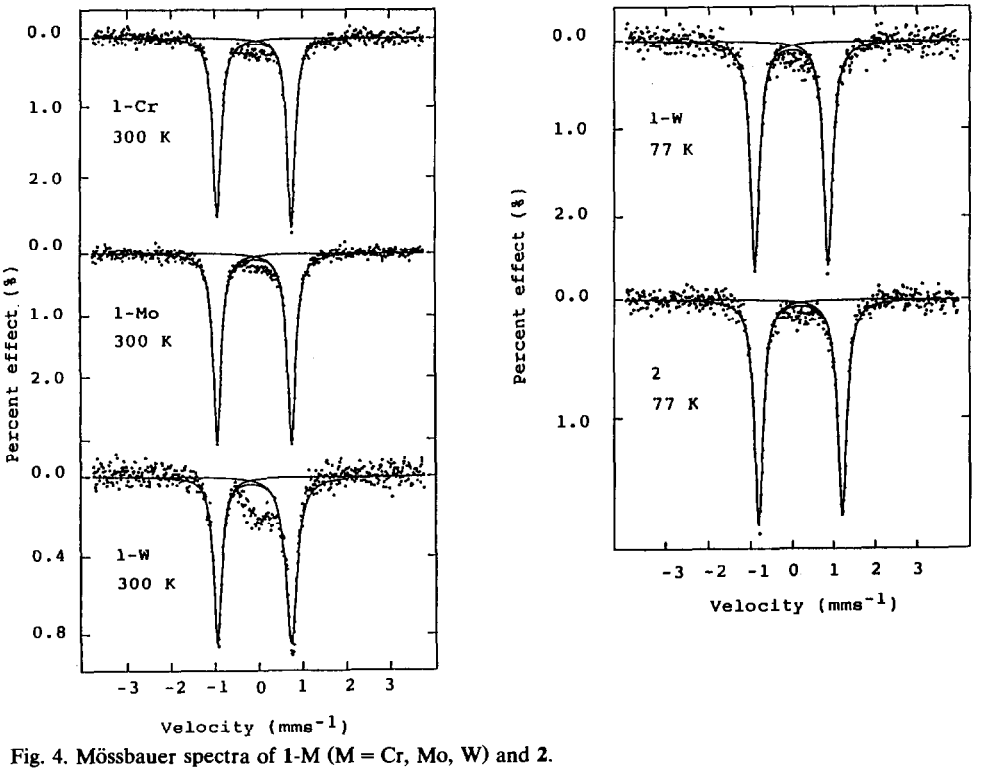

Fig. 4. Mössbauer spectra of **1**-M (M = Cr, Mo, W) and **2**.

TABLE 6. ^{59}Fe Mössbauer least-squares-fitting parameters for complexes 1-M (M = Cr, Mo, W) and 2

Compound	T, K	ΔE_Q, mm/s	δ, [a] mm/s	Γ, [b] mm/s
1-Cr	300	1.6828	0.0081	0.2163, 0.2302
1-Mo	300	1.6864	0.0088	0.2324, 0.2174
1-W	300	1.672	−0.0011	0.3030, 0.2199
	77	1.7692	0.0797	0.2597, 0.2577
2	77	2.0197	0.2914	0.2669, 0.2518

[a] Isomer shifts. [b] Full width at half-height taken from the least-squares-fitting program. The width for the line at more positive velocity is listed first for each doublet.

equilibrium with **B'**, is the major species. Because of the exchange of the four *cis* tungsten CO via the rotation of the P–W bond, we could only observe a hump in the ^{13}C NMR spectrum at room temperature.

3.3. Mössbauer spectra of 1-M (M = Cr, Mo, W) and 2

Figure 4 shows the Mössbauer spectra of **1**-Cr, **1**-Mo and **1**-W obtained at 300 K. The absorption peaks in each spectrum were fitted to Lorentzian lines, and the resultant fitting parameters are summarized in Table 6. Isomer shifts of these compounds were of the same order within the limits of experimental error. This indicates the similarity of the influences of different (μ-PPh$_2$)M(CO)$_5$ (M = Cr, Mo, W) fragments on the Fe moiety. The reason for the small hump observed in the Mössbauer spectra of **1**-W at room temperature was not clear. The presence of impurities in the sample was excluded because we did not observe the hump when the spectrum of this sample was taken at 77 K.

The Fe–W bond in **2** may serve as a dative bond to donate two electrons to the Fe atom. It would be of interest to realize the influence on Fe when one of its CO ligands in **1**-W was replaced by the metal dative bond (*cf.* **2**). Mössbauer spectra of **1**-W and **2** taken at 77 K are shown in Fig. 4. Isomer shift increased from 0.0797 in **1**-W to 0.2914 m ms^{-1} in **2** at 77 K (Table 6). Because the dative metal–metal bond is not a π acceptor, the replacement of the CO in **1**-W by the dative metal–metal bond to form **2** may increase the d shielding orbital electron density on the Fe atom. This should result in an increase of isomer shift. Nevertheless, the semibridging CO which was formed by donating d electron density from the Fe atom to the π^* orbital of the CO ligand reduced the shielding d electrons of the Fe atom. Thus a decrease of isomer shift should be observed. Our Mössbauer results indicate that the former factor dominated. This phenomenon was also reported in the case of CpFe(CO)$_2$(μ-PPh$_2$)Fe(CO)$_4$ (**3**) and CpFe(CO)(μ-CO)(μ-PPh$_2$)Fe(CO)$_3$ (**4**) [20]. The former possesses a smaller isomer shift (0.09 m ms^{-1}) than the latter (0.19 m ms^{-1}).

Acknowledgments

For financial support, we gratefully acknowledge National Science Council (through Grant NSC82-0208-M001-63) and Academia Sinica.

References and notes

1 (a) R.J. Haines, C.R. Nolte, R. Greatrex and N.N. Greenwood, *J. Organomet. Chem., 26* (1971) C45; (b) W. Ehrl and H. Vahrenkamp, *J. Organomet. Chem., 63* (1973) 389.
2 R.J. Haines, C.R. Nolte, *J. Organomet. Chem., 36* (1972) 163.
3 (a) E. Lindner, M. Heckmann, R. Fawzi and W. Hiller, *Chem. Ber., 124* (1991) 2171; (b) P. Braunstein, E. de Jesus, A. Tiripicchio and M.T. Camellini, *J. Organomet. Chem., 368* (1989) C5; (c) S. Guesmi, P.H. Dixneuf, G. Suss-Fink, N.J. Taylor, A.J. Carty, *Organometallics, 8* (1989) 307; (d) J. Powell, J.F. Sawger and M.V.R. Stainer, *Inorg. Chem., 28* (1989) 4461; (e) E. Lindner, M. Stangle, W. Hiller and R. Fawzi, *Chem. Ber., 121* (1988) 1421; (f) S. Guesmi, P.H. Dixneuf, N. Taylor and A.J. Carty, *J. Organomet. Chem., 328* (1987) 193; (g) S. Guesmi, N.J. Taylor, P.H. Dixneuf and A.J. Carty, *Organometallics, 5* (1986) 1964; (h) D.A. Roberts, G.R. Steinmetz, M.J. Breen, P.M. Shulman, E.D. Morrison, M.R. Duttera, C.W. DeBrosse, R.R. Whittle and G.L. Gerffroy, *Organometallics, 2* (1983) 846.
4 (a) H. Vahrenkamp, *J. Organomet. Chem., 63* (1973) 399; (b) W.T. Osterloh. PhD Thesis, University of Texas, Austin, TX, 1982. University Microfilms International, Ann Arbor, MI 1982.
5 (a) R.A. Jones, J.G. Lasch, N.C. Norman, A.L. Stuart, T.C. Wright and B.R. Whittlesey, *Organometallics, 3* (1984) 114; (b) D.J. Chandler, R.A. Jones, A.L. Stuart and T.C. Wright, *Organometallics, 3* (1984) 1830; (c) H.A. Jenkins, S.J. Loeb, and D.W. Stephan, *Inorg. Chem., 28* (1989) 1998.
6 S.G. Shyu, P.J. Lin and Y.S. Wen, *J. Organomet. Chem., 443* (1993) 115.
7 J.F. Lee, M.D. Lee and P.K. Tseng, *Hua Hsueh, 45* (1987) 50.
8 Equation of the plane: $-0.182(18)x + 13.857(12)y - 8.968(13)z = 1.387(7)$. Distances to the plane from the atoms in the plane: P −0.0009(20), C4 −0.019(7), C5 0.018(8), C3 0.015(7) Å. Chi squared for this plane 16.422. Distances to the plane from the atoms out of the plane: W 0.004(3), Fe 0.442(5) Å.
9 J.C. Jeffery and J.G. Lawrence-Smith, *J. Chem. Soc., Dalton Trans.*, (1990) 1063.
10 J.C. Jeffery and J.G. Lawrence-Smith, *J. Chem. Soc., Dalton Trans.*, (1990) 1589.
11 J.C. Jeffery, K.A. Mead, H. Razay, F.G.A. Stone, M.J. Went and P. Woodward, *J. Chem. Soc., Chem. Commun.*, (1981) 867.
12 J. Hein, J.C. Jeffery, P. Sherwood and F.G.A. Stone, *J. Chem. Soc., Dalton Trans.*, (1987) 2211.
13 J.C. Jeffery, M.J. Parrott and F.G.A. Stone, *J. Chem. Soc., Dalton Trans.*, (1988) 3017.
14 Equation of the plane: $9.036(15)x - 1.34(10)y - 6.17(11)z = 1.77(14)$. Distances to the plane from the atoms in the plane: P −0.003(9), C4 −0.11(4), C5 0.05(3), C3 0.06(4) Å. Chi squared for this plane 13.056. Distances to the plane from the atoms out of the plane: W 0.035(13), Fe 0.416(20) Å.
15 W.C. Mercer, R.R. Whittle, E.W. Burkhardt and G.L. Geoffroy, *Organometallics, 4* (1985) 68.

16 F.-E. Baumann, J.A.K. Howard, O. Hohmnson, and F.G.A. Stone, *J. Chem. Soc., Dalton Trans.*, (1987) 2917.
17 F.A. Cotton, *Progr. Inorg. Chem., 21* (1976) 1.
18 IR spectrum of complex **2** (CH_2Cl_2, ν(CO)): 2056m, 1958s, 1927m cm^{-1}.
19 (a) A.J. Carty, S.A. MacLaughlin and D. Nucciarone, in J.G. Verkade, L.P. Quin (Eds.), *Phosphorus-31 NMR Spectroscopy in Stereochemical Analysis. Organic Compounds and Metal Complexes*, VCH Publisher: New York, 1987. Chapter 16, and references cited therein; (b) A.J. Carty, *Adv. Chem. Ser., 196* (1982) 163; (c) D.E. Garron, *Chem. Rev., 81* (1981) 229.
20 R. Greatrex and R.J. Haines, *J. Organomet. Chem., 114* (1976) 199.